GeoScienceWorld
Lithosphere
Volume 2022, Article ID 2904927, 17 pages
https://doi.org/10.2113/2022/2904927

Lithosphere

Research Article

Analysis of Temporal and Spatial Evolution Characteristics of Land Subsidence in Western Songnen Plain Using Multisource Remote Sensing

Lianjing Zheng,[1] Qing Wang,[1] Zeyu Wang,[1] Fengyan Wang,[2] and Chen Cao [1]

[1]*College of Construction Engineering, Jilin University, Changchun, Jilin 130026, China*
[2]*College of Geo-Exploration Science and Technology, Jilin University, Changchun, Jilin 130026, China*

Correspondence should be addressed to Chen Cao; ccao@jlu.edu.cn

Received 18 April 2022; Accepted 23 May 2022; Published 11 June 2022

Academic Editor: Manchao He

The exploitation of underground fluid is an important factor leading to land subsidence. The effects of mining depth, frequency, and mode on land subsidence are also different. The objective of this study was to develop a multisource method—including optical remote sensing interpretation, Interferometric Synthetic Aperture Radar (InSAR) technology, and unmanned aerial vehicle (UAV)—to reveal the long-term temporal and spatial evolution law of subsidence characteristics driven by groundwater and oil extraction, as well as to reveal the formation mechanism and seasonal response law of land subsidence under the action of different driving factors. In this paper, we select the western region of Jilin Province located in Songnen Plain as the study area. The subsidence funnels in the study area are distributed in a porphyritic manner, and the distribution of the subsidence funnels has a certain correlation with the distribution of the pumping wells. In farmland areas, the subsidence is mainly caused by pumping groundwater. The annual land subsidence rate in the study area is -3.14 mm/a, and the maximum deformation rate in the study area is -22.05 mm/a. The subsidence is affected by the season, shown by the fact that it rises in the dry season and decreases in the rainy season. The subsidence in the west of Songnen Plain is caused by oil pumping and groundwater pumping, and groundwater pumping is dominant. The exploitation of underground fluid transfers the pressure borne by water or oil to the soil skeleton so as to increase and consolidate the effective stress of the soil layer and lead to land subsidence. The continuous observation of the surface in the western area of Songnen Plain is helpful to guide the safe production of agriculture and industry and ensure the smooth development of local industry and agriculture.

1. Introduction

As a common geological disaster all over the world, land subsidence is generally caused by a series of natural and human factors, in which human activities are dominant [1]. The land subsidence caused by such factors is very slight in the initial stages and difficult to measure, but in the medium term, the subsidence intensifies and the scope of influence expands, resulting in huge harm, damage to ground facilities, and may induce earthquakes in serious cases.

With the development of humankind, the problem of land subsidence is becoming more and more serious. More and more technical means and theoretical models are applied for the prevention and control of land subsidence. At present, there are many studies in theoretical models and numerical simulations, including the seepage field model [2], stress field model [3], and coupling simulation [4]. Monitoring methods for land subsidence include deformation meter [5] and GNSS [6]. These methods have the characteristics of high measurement accuracy and simple operation. However, these monitoring methods also have some shortcomings, such as limited monitoring points and only macroscopic observation of land subsidence characteristics. They are not suitable for large-area and automatic monitoring, and it is difficult to accurately grasp the overall distribution characteristics of subsidence [7].

Interferometric Synthetic Aperture Radar (InSAR) uses a variety of analysis methods to process radar images, which can obtain the surface elevation and micro deformation information of the target area [8], and this method has great advantages in monitoring regional surface deformation. Massonnet first used Differential Interferometric Synthetic Aperture Radar (D-InSAR) to obtain the settlement of the Landers earthquake in 1993 [9]. Since then, a series of InSAR time series analysis methods have been widely used in the monitoring process of land subsidence, such as Persistent Scatterer Interferometric Synthetic Aperture Radar (PS-InSAR) [10] and Stanford Method for Persistent Scatters (StaMPS) [11]. Some scholars also use InSAR to monitor the areas of land subsidence caused by different factors and analyze the possible causes of subsidence in combination with corresponding models and data [12, 13]. The small baseline set technology (SBAS-InSAR) has the advantages of obtaining small deformation information and long-time series of slow surface deformation [14]. In recent years, it has been widely used in deformation monitoring of landslide [15, 16], land subsidence [17, 18], debris flow [19], and volcanic activity [20, 21]. SBAS-InSAR technology has been successfully used to monitor and analyze land subsidence in Beijing [22], Suzhou [23], Semarang [24], Tianjin [25], Lagos [26], and other places. In oilfield areas [27, 28], it shows high accuracy and reliability.

In the oil field area in particular, the land subsidence may be caused by a variety of factors. For example, a large oil field in the Zagros fold thrust belt in southwest Iran may be comprehensively affected by tectonic activity, underground pressure reduction, hydraulic fractures, reservoir rock physical properties, and oil production [29]. A large number of studies have attributed the main cause of land subsidence to the exploitation of underground fluid [30–32]. In most areas, the groundwater level will decline and with the exploitation of groundwater, which will increase the effective stress of the relevant soil layers and consolidate the soil layer, thus causing land subsidence. The formation mechanism of land subsidence caused by oil and gas exploitation is similar to that of groundwater exploitation. However, in the process of oil and gas field exploitation, a large amount of water is needed to inject water into the reservoir, and groundwater will be extracted during this period. Pumping oil will lead to land subsidence, and the groundwater injected in order to improve oil recovery will also lead to land uplift or uplift [33]. Therefore, in the study of oilfield surface subsidence, both pumping and oil pumping can dominate land subsidence [34]. In most cases, oilfield subsidence may not have a significant impact on surface structure [35]. However, oilfield subsidence will affect the local ecological environment, underground hydrological system, and surface drainage pattern for a long time [36] and indirectly affect land subsidence through other factors. Therefore, there is a high correlation between land subsidence and groundwater extraction, oil, and gas fields in time and space [37].

The saline land area in western Songnen Plain is the frontier of the national strategic project "land consolidation in Western Jilin." In the process of preliminary research, whether its development direction poses a threat to existing projects and creates engineering disasters is worthy of further discussion and research. Oil and gas exploitation and groundwater extraction can easily lead to land subsidence. Land subsidence is a slow and imperceptible geological disaster phenomenon in its early stages, which brings about many hazards to the subsidence area, such as the destruction of underground pipelines, roads, and railways, and causes many secondary disasters at the same time. In addition, it affects the normal operation of the national strategic project "land consolidation in Western Jilin" and the water diversion project, endangers the ecological environment in Western Jilin, and restricts the normal evolution of Western Jilin. The intensification of land subsidence and ecological environment change in the west of Jilin Province has attracted great attention from many scholars.

The innovation of this paper is to use multisource data to reveal the characteristics of land subsidence caused by different driving factors. InSAR technology can be used to realize the monitoring and feature analysis of large areas and long time series. High-resolution optical remote sensing images can not only identify the deformed areas but also conduct a large-scale investigation of the ground features in the study area. The UAV aerial survey can carry out high-precision measurement and can observe the settlement deformation more carefully and intuitively. The characteristics of land subsidence in this area are discussed by combining multisource data.

The objectives of this study are to discuss the characteristics of land subsidence in the western area of Songnen Plain and analyze the relationship between land subsidence and the exploitation of groundwater and oil by using optical remote sensing, InSAR technology, and UAV aerial survey. The main purposes of this study are as follows: (1) to clarify the distribution characteristics and laws of land subsidence in Qian'an oilfield and its surrounding areas in western Songnen Plain, finding out the spatial relationship between land subsidence and oil wells; (2) to reveal the long-term temporal and spatial evolution law of typical subsidence areas and clarify the spatial deformation characteristics of land subsidence funnels under the action of different driving factors; and (3) to reveal the formation mechanism and seasonal response law of land subsidence under the action of different driving factors. Using multisource data to analyze the land subsidence in the study area, we summarize the main causes of land subsidence, providing ideas and suggestions for the analysis of similar land subsidence.

2. Geological Settings

The study area is located in 123° 55′ 20″ E-124° 23′ 04″ E, 45° 05′ 20″ N-44° 47′ 57.02″ N, and the area is about 1209.64 km^2. The study area belongs to an alluvial plain landform, which is located in the northwest of Jilin Province (Figure 1). The overall terrain is flat, slightly higher in the southwest and lower in the northeast. The geological structure belongs to Songliao Basin, which was formed in the late Jurassic (J) and early Cretaceous (K) eras. The study area is a

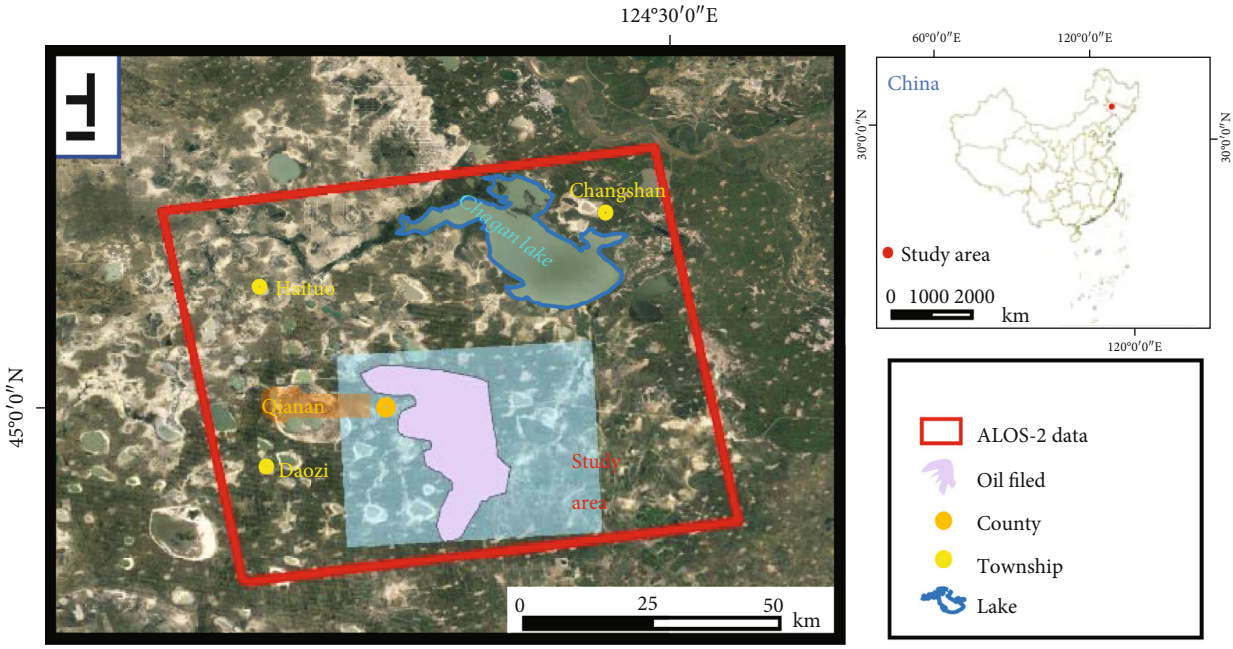

Figure 1: Location and geomorphological of study area.

part of the Mesozoic and Cenozoic Songliao giant fault basin, bounded by the Qianguo–Changling line, forming the eastern uplift belt and the central depression belt, generally depositing the quaternary system with a thickness of 80-120 m, including platform formation (Q_1), Huangshan formation (Q_2^1), Daqinggou formation (Q_2^2), and Guxiangtun formation (Q_4). The underlying system is Neogene, including Miocene Daan formation (N_d), Pliocene Taikang formation (N_t), and Neogene Pliocene to Quaternary lower Pleistocene (N_2^2-Q_1) Baitushan formation. The Mesozoic strata in the basin are relatively developed, in which Jurassic (J) is siltstone, mudstone, and volcanic rock with thin coal. The stratum includes multiple cycle layers composed of conglomerate, sandstone, and shale and is rich in oil resources, such as in Qian'an oilfield and Daqingzijing oilfield.

The study area is dry and windy in spring and autumn, hot in summer, and cold in winter, belonging to a temperate semiarid continental monsoon climate. The annual average temperature in the study area is 5.6°C, and the average annual precipitation is 425.8 mm. The rainy season is from May to September. The average precipitation in the rainy season can reach 413.37 mm. The precipitation is concentrated in summer and significantly lower in winter. The annual evaporation far exceeds the rainfall, which is 1849.01 mm. The groundwater in the area is composed of a pore phreatic aquifer and three overlapping confined water aquifers and is rich in groundwater resources, while the surface water resources are poor, mainly the exploitation of groundwater.

3. Data and Methods

3.1. Small Baseline Subset Interferometric Synthetic Aperture Radar (SBAS-InSAR). The data selected for this study include the L-band ALOS-2 PALSAR data of Japan Space Agency (Figure 1). The satellite has the characteristics of strong penetration, antiloss of coherence, and penetrating clouds [38]. It is widely used in the monitoring of landslides, land subsidence, earthquakes, and other geological hazards. The data are obtained along the same track descending direction, and the time span is from November 21, 2014 to October 18, 2019. There are 13 periods of data in total. SBAS-InSAR is a new time series analysis method, which uses short interference to overlay and analyze the track image (Figure 2(a)). In order to extract the surface deformation information for the purpose of efficient and accurate monitoring, a DEM (Digital Elevation Model) of 30 m Shuttle Radar Topography Mission Digital model (30 m SRTM DEM) was used for topographic reference.

There are 13 periods of data during this period (Table 1). These data are processed by SBAS-InSAR method to obtain ground deformation data. SBAS-InSAR was proposed by Berardino et al. [39]. This method can further realize long time series and millimeter-level monitoring on a regional scale. By processing N+1 SAR images in the same area, we select one as the main image, register the other images to the main image, set a reasonable threshold to generate a difference image to improve the interference of the interferogram, and then obtain the nonlinear deformation of the time series by using the methods of phase unwrapping, filtering, and singular value decomposition. This can effectively solve the problems of discontinuous and sparse time sampling so as to obtain higher spatial resolution, overcome the limitations of time and space decorrelation and atmospheric effect in traditional InSAR, reduce the demand for SAR data, and improve its operation efficiency. According to the image data and topographic features obtained in the study area, the steps of data processing mainly include data

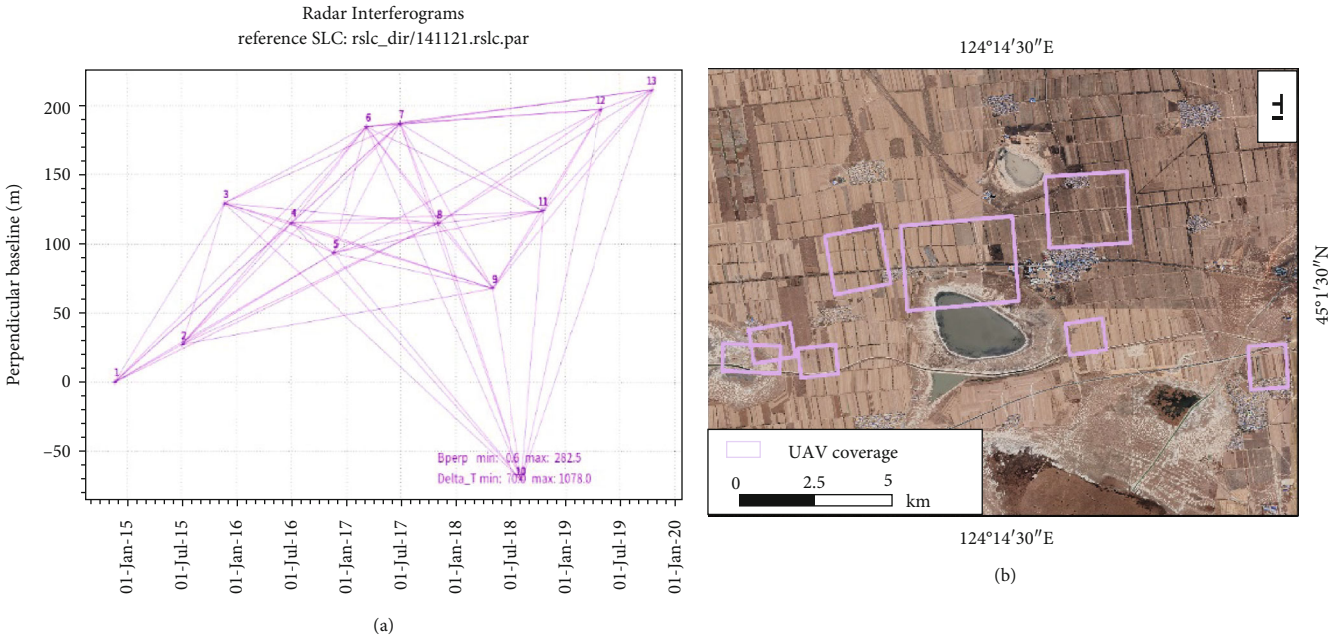

Figure 2: (a) Perpendicular baseline; (b) UAV coverage.

Table 1: Data list of ALOS-2 in study area.

Serial number	Imaging time	Polarization mode	Cumulative time baseline (/d)
1	20141121	HH	0
2	20150703	HH	224
3	20151120	HH	394
4	20160721	HH	637
5	20161118	HH	757
6	20170310	HH	869
7	20170630	HH	981
8	20171103	HH	1107
9	20180504	HH	1300
10	20180810	HH	1398
11	20181019	HH	1468
12	20190503	HH	1664
13	20191018	HH	1836

conversion to generate a connection map, differential interference to generate an interferogram, phase unwrapping, orbit refining and releveling, and then inversion and geocoding of the obtained interferogram. The processing flow chart of SBAS-InSAR is shown in Figure 3.

3.2. Unmanned Aerial Vehicle High-Resolution Optical. As a popular approach in remote sensing technology, unmanned aerial vehicle (UAV) can quickly and accurately obtain high-precision data in the study area. The UAV is used to carry out multistage photogrammetric observation on eight typical areas in the study area, which is compared with the results interpreted by SBAS-InSAR technology, especially to observe the impact of irrigation season on the surface in the study area (Figure 2(b)). According to the surface conditions in different regions, the UAVs selected in this study are DJI M300 and DJI spirit 4. The eight typical areas photographed are mainly near Rangzi town. They flew for four periods in March, April, May, and August in 2021, respectively. The flight altitude is 300 m, and the total flight area is 57.95 km^2 in total, obtaining 8734 photos. Through image processing and other operations, the regional DEM, DOM (Digital Orthophoto Map), DSM (Digital Surface Model), and other data are obtained for interpretation comparing with InSAR interpretation results. Using UAV high-resolution optical, DEM, DSM, and DOM with a resolution of 3 cm and accuracy of 1.5 cm can be obtained.

Using InSAR technology can realize the preliminary judgment of a large-scale regional settlement funnel, while for the surface situation in the study area, high-resolution remote sensing images and UAV high-resolution optical need to be used. In this paper, the distribution of surface pumping wells in the study area is interpreted by using a 1.69 m resolution optical remote sensing image. As the water well is small and difficult to interpret by remote sensing image, the UAV high-resolution optical was used for measurement, and the position distribution of the water well was interpreted using the UAV high-precision image.

4. Results

In this study, we used several investigation techniques, including InSAR, optical remote sensing interpretation, and UAV mapping, to identify and analyze the land subsidence in the typical area of Western Songyuan Plain. SBAS-InSAR technology can help us realize the analysis of surface deformation in a large scale and can target and obtain the areas that need typical verification. Therefore, the large-scale census using InSAR techniques is very

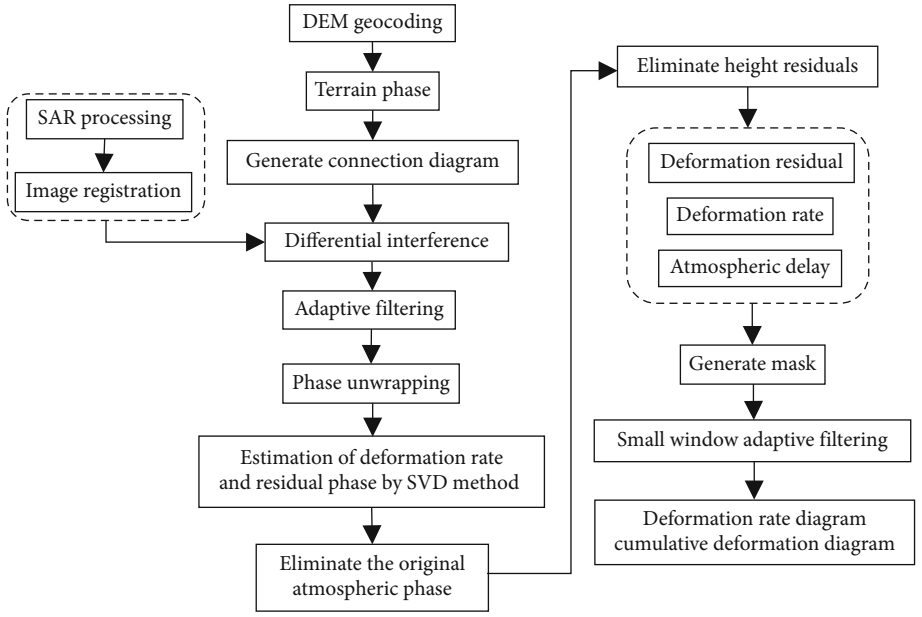

Figure 3: SBAS-InSAR processing flow chart.

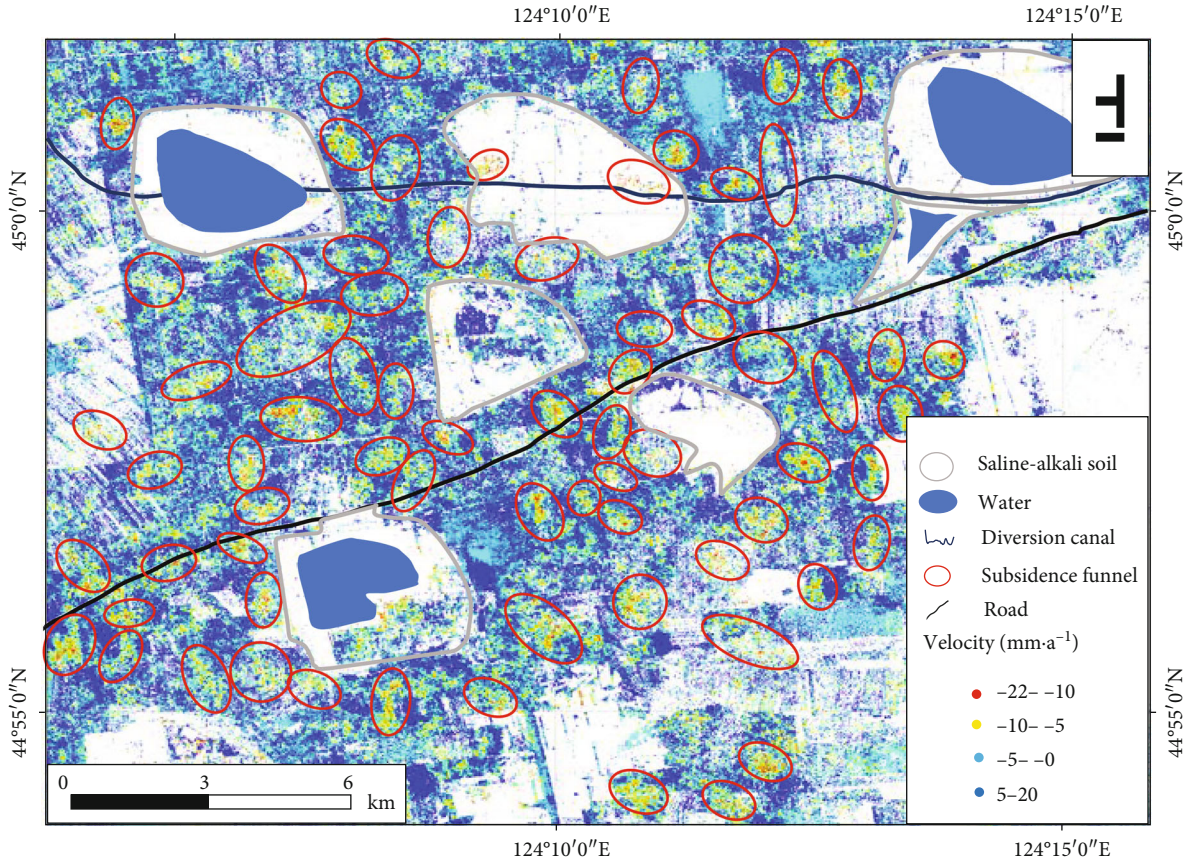

Figure 4: Ground deformation velocity map of the study area.

necessary. However, the resolution of the ALOS-2 data is only 10 m, and the fine deformation characteristics of the surface are difficult to be identified by InSAR. It is necessary to realize the fine analysis of surface deformation through high-resolution differential observation, and high-resolution UAV mapping can achieve this goal. Therefore, according to

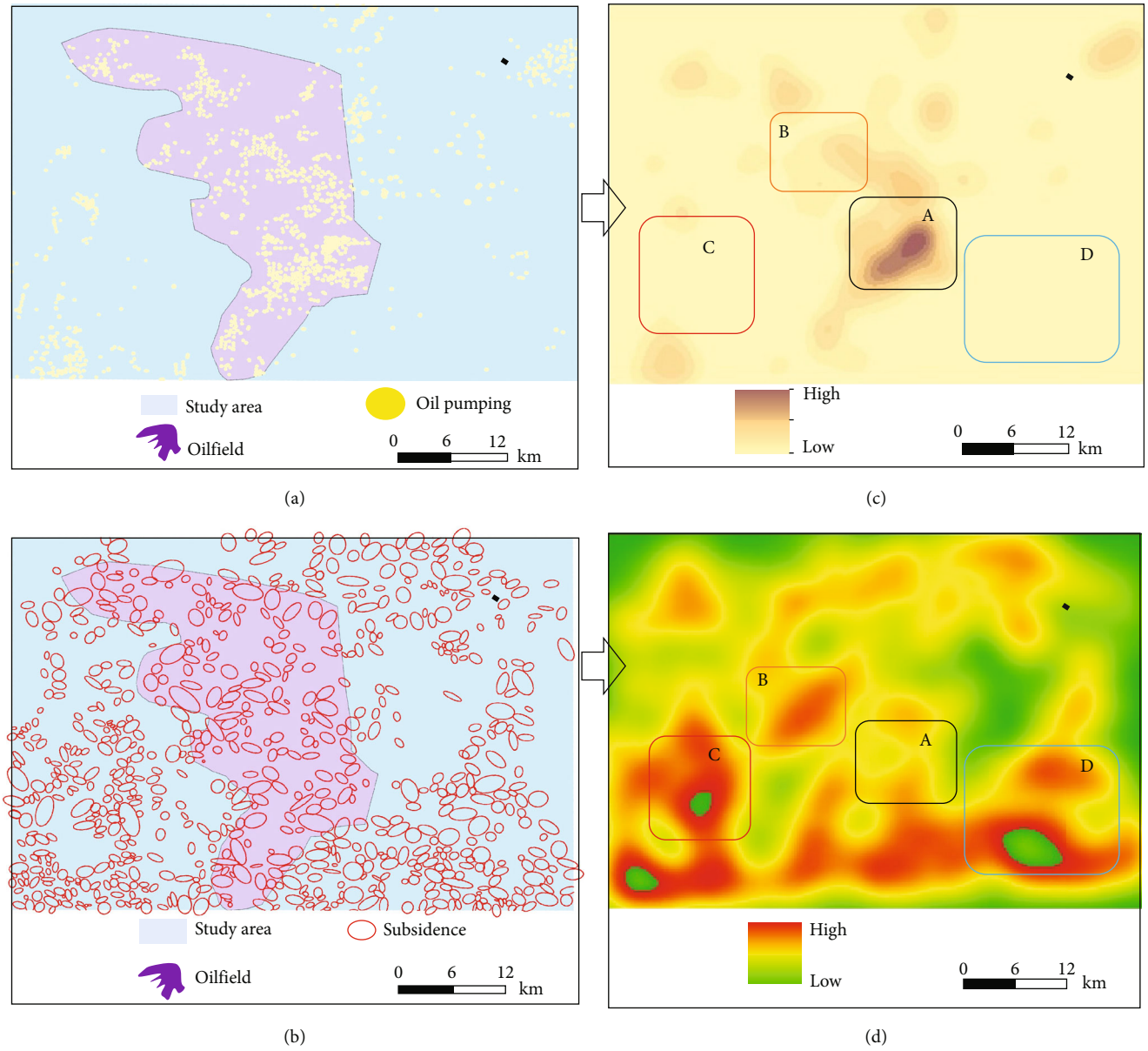

Figure 5: Distribution of oil pumping, subsidence, and their kernel density: (a) oil pumping; (b) subsidence funnels; (c) kernel density of oil pumping; (d) kernel density of subsidence funnels.

the interpretation results of InSAR, we select typical areas of farmland and oil wells, selecting eight areas for UAV aerial photography and two typical areas for elaboration.

4.1. Subsidence Spatial Pattern. SBAS-InSAR is used to extract the surface deformation features of ALOS images covering the study area and to obtain the annual average surface velocity along the line of sight of satellite radar. In Figure 4, the blue positive value represents growth of land deformation, that is, land uplift. Additionally, the red negative value represents the negative growth of land deformation, that is, land subsidence. On the whole, the data coverage is good, and the coherence is high. The results show that the subsidence occurs widely in the study area, and this subsidence is distributed in a patchy pattern. There is no large-area overall deformation. A total of 747 subsidence funnels are circled. Most of them are oval or approximately circular in shape, with different areas. The speed change rate of land subsidence gradually increases from the outside to inside, which corresponds with the characteristics of land subsidence funnel. The overall annual land subsidence rate in the study area is -3.14 mm/a. Assuming that the ground uplift is negligible, the rate range of each land subsidence funnel is 0-15.14 mm/a. The maximum deformation rate in the study area is -22.05 mm/a. However, due to the constraints of scatter changes, radar wave transmittance, and other factors, incoherence occurs around and in a lake area, with no coherent points.

Seen from Figure 5, there is a large area of oilfields in the study area. Through the interpretation using the remote

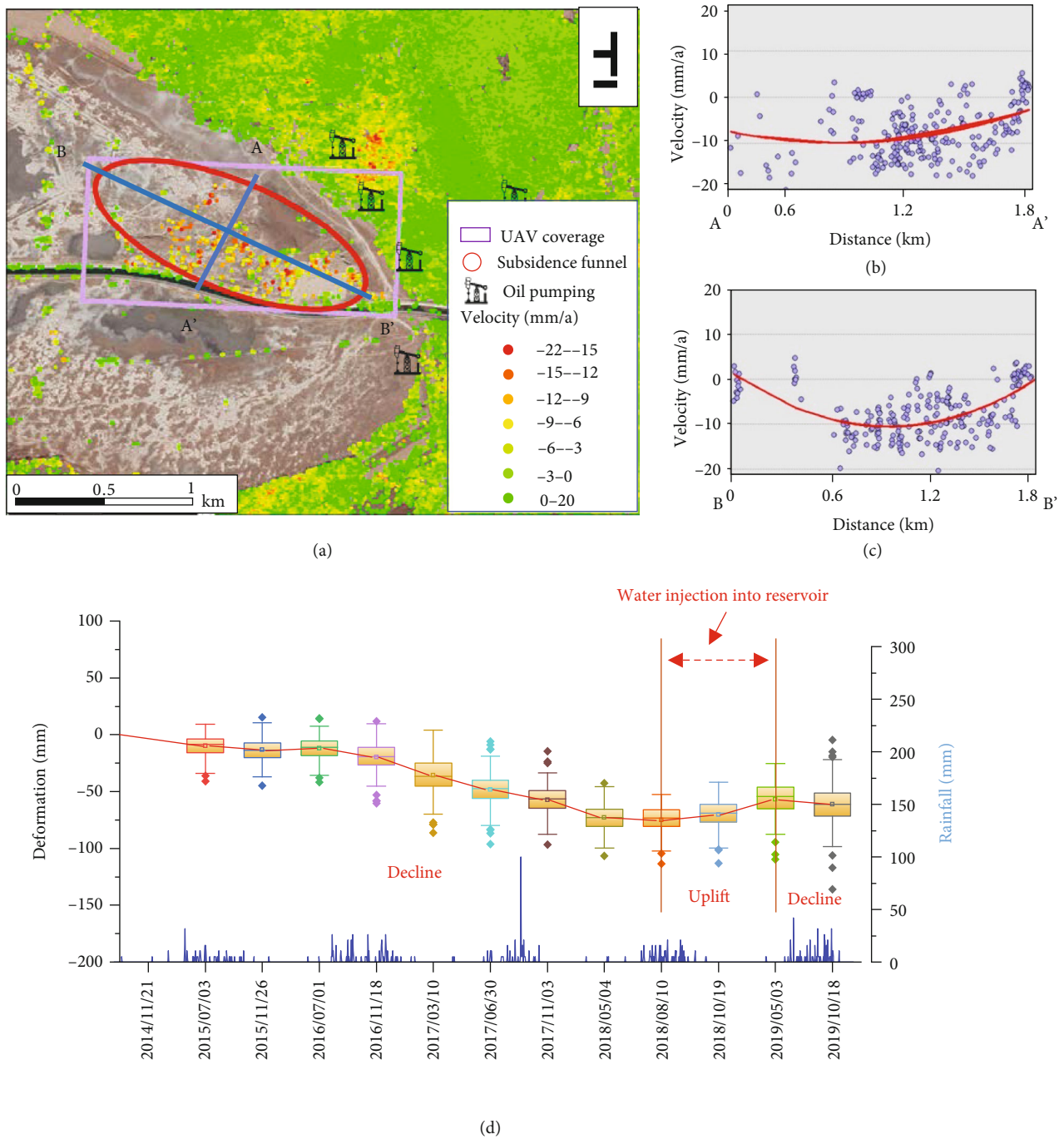

Figure 6: Subsidence characteristics of typical oilfield: (a) subsidence velocity map in oilfield; (b) A-A' profile; (c) B-B' profile; (d) subsidence box diagram.

sensing images of Google Earth, the location and scope of pumping wells are preliminarily delineated, and 1275 pumping wells are delineated. From the interpretation results, the distribution range of pumping wells is basically consistent with that of oilfields. The InSAR results show that the land subsidence in the study area is distributed in a patchy manner, shown in Figure 5, and the location of the pumping wells can be observed near most land subsidence areas, especially in the oilfield area. In addition, the long-term extraction of groundwater resources in farmland areas will also cause land subsidence to varying degrees. Therefore, there is land subsidence distributed in spots in nonoilfield areas, i.e., farmland.

The distribution range of oil wells interpreted by remote sensing is basically consistent with the boundary of Qian'an oilfield (Figures 5(a) and 5(b)). The density of oil wells in the south of the oilfield (zone A and zone B) is large, and there is still a small amount of distribution outside the oilfield

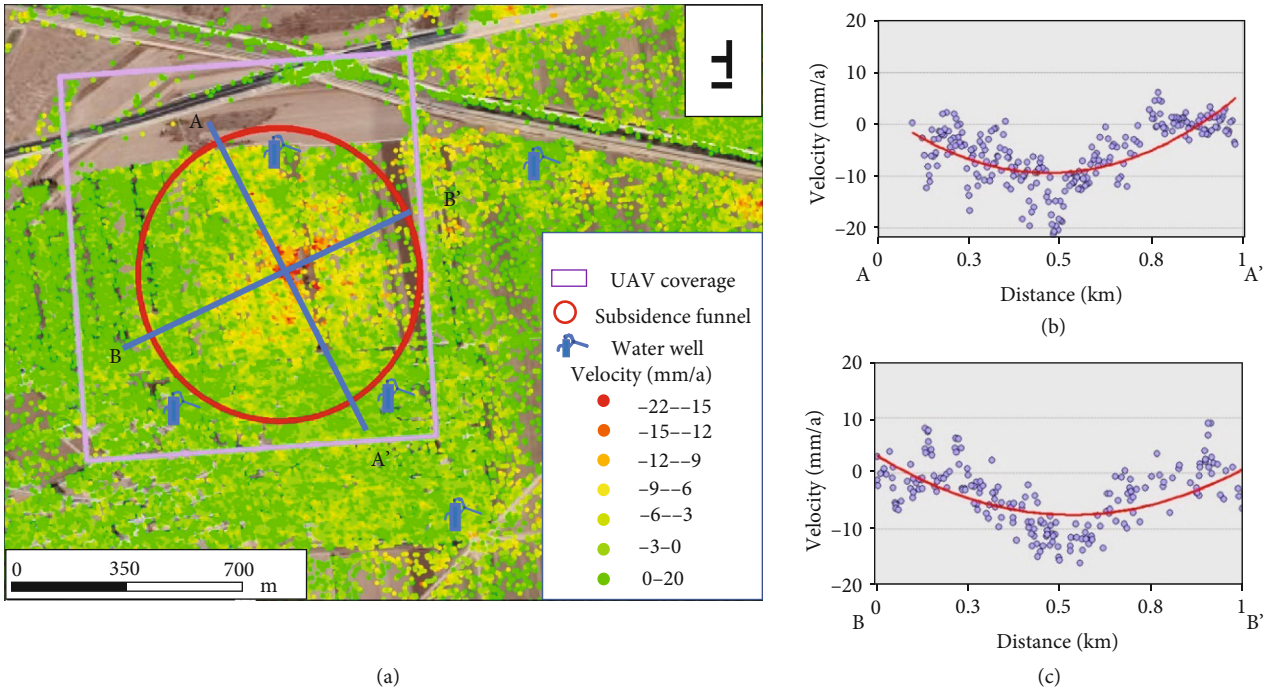

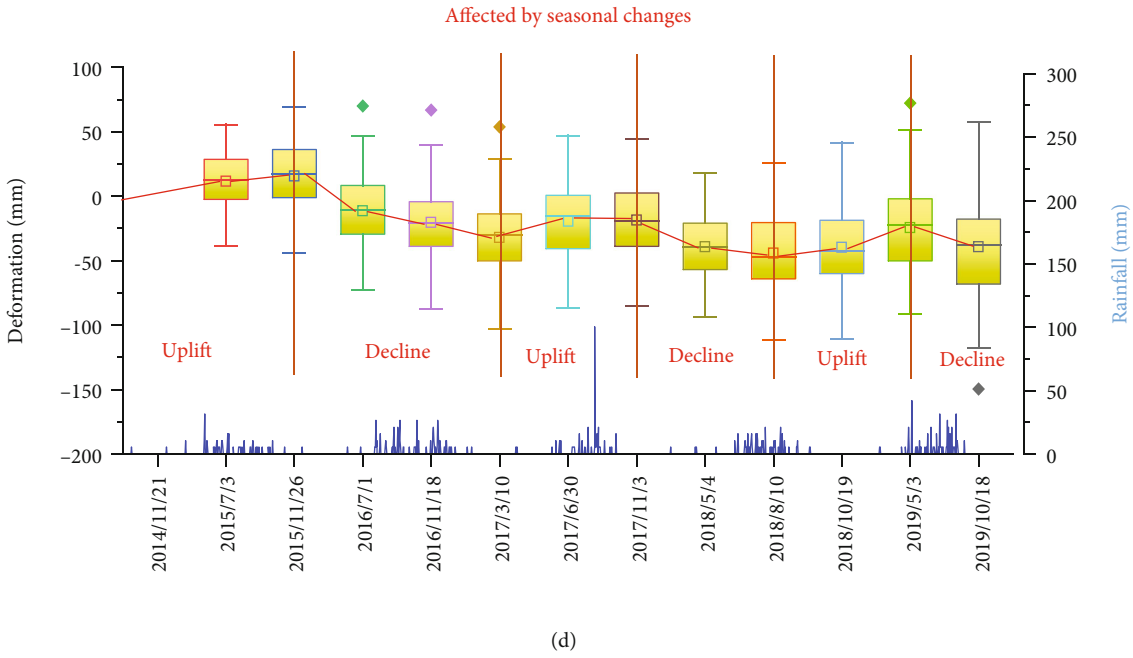

FIGURE 7: Subsidence characteristics of typical farmland: (a) subsidence velocity map in oilfield; (b) A-A' profile; (c) B-B' profile; (d) subsidence box diagram.

boundary. The density of oil wells in zone A is the largest, but the density of subsidence funnels in zone A is very low. The distribution density of oil wells in zone B is also relatively large, and the density of subsidence funnels is also relatively high. There are basically no oil wells in zone C and zone D, but Figure 5(d) shows that there are many subsidence funnels in zone C and zone D, which are densely distributed. According to remote sensing interpretation, these areas are farmland areas. Therefore, it can be seen that the farmland and oilfield areas in the study area have a large density of subsidence funnel distribution. Oil pumping and groundwater pumping will lead to different degrees of land subsidence, in which the proportion of farmland settlement funnel is large, and the distribution density is also large. The study area comprises mainly farmlands, and the extraction of groundwater may be the main driving factor of land subsidence.

4.2. Temporal Evolution. In order to clarify the evolution law of surface deformation in the study area in time series,

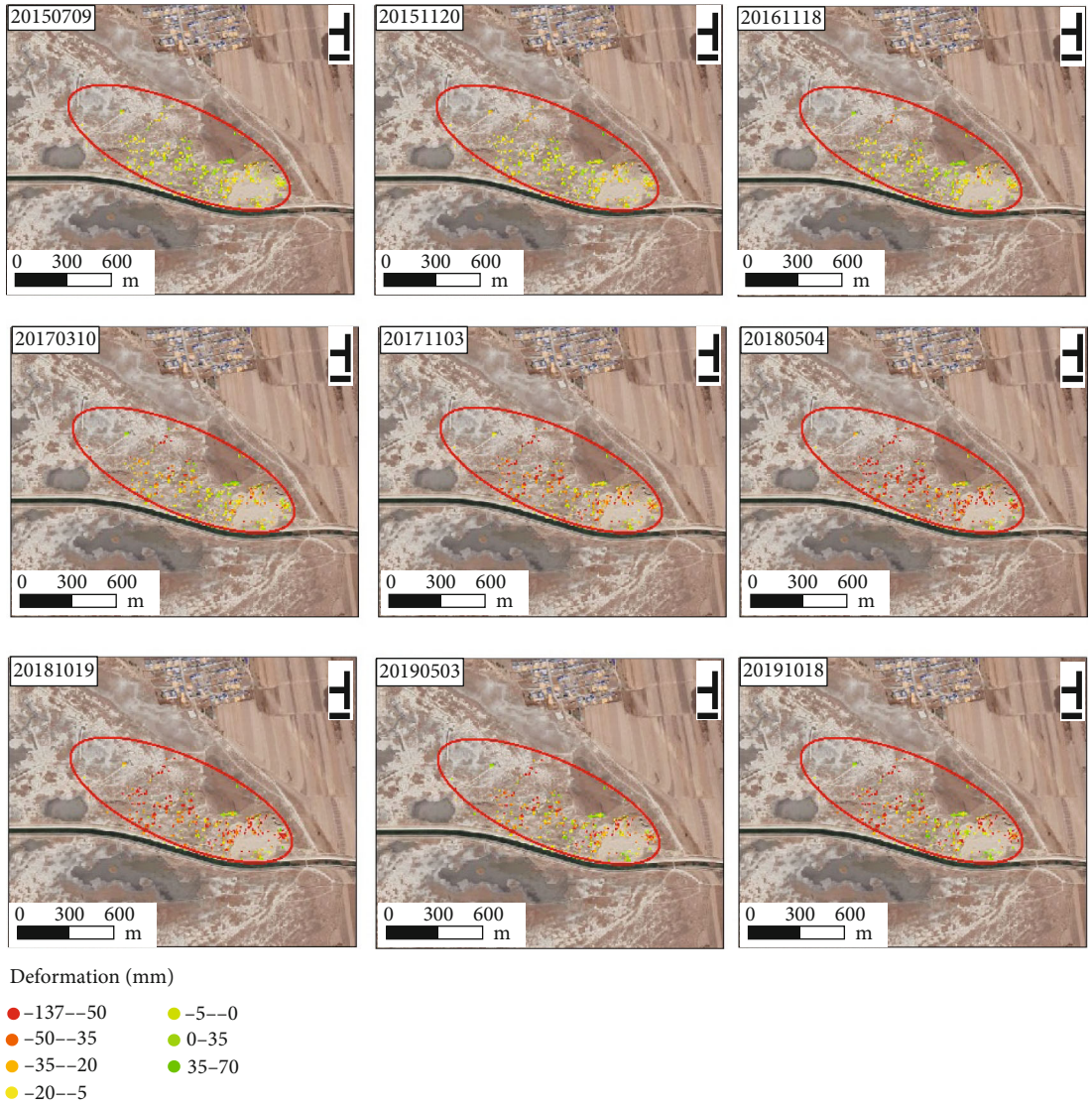

Figure 8: InSAR deformation map of farmland regional time series.

typical land subsidence areas are selected for time-series analysis at the locations of oilfields and farmland (Figures 6 and 7). From November 21, 2014 to October 18, 2019, the ground surface of the study area experienced a process from subsidence to uplift and then back to subsidence, but the subsidence features are different in different regions, indicating that the main reasons for land subsidence are different and the mechanisms are also different.

Figure 6(d) is a sequence variation box diagram of deformation at the oilfield. These data are considered combined with rainfall. It is found that there are three periods from subsidence to uplift since the data recording day. The period of subsidence is longer than that of surface uplift, and the deformation variables of subsidence are more than those of uplift. The overall surface is in a state of downward subsidence and deformation. The subsidence period on July 1, 2016 is the longest, and this subsidence lasted until August 10, 2018. The subsidence time lasted for 771 days, after which the surface began to uplift. The seasonal change in this area is not obvious. The rainy season lasts from May to September every year, and the dry season is from October to April of the next year. However, subsidence occurred in the rainy seasons of 2015, 2016, and 2017. In particular, the strongest rainfall in the last five years was from May to September 2017, which kept the state of subsidence until the next year. This feature is also illustrated by the InSAR timing variation diagram of this area in Figure 8. As of August 10, 2018, the settlement deformation of the oilfield area has increased year by year, but since then, the surface elevation has recovered until October 18, 2019.

Figure 7(d) is the time-series box diagram of farmland area. From the deformation observed from November 21, 2014 to October 18, 2019, the land has experienced three processes from uplifting to settlement. Compared with the period of subsidence and uplift, there is no continuous subsidence for several consecutive years in the oilfield area, but there are more regular changes. The surface deformation is affected by seasonal changes. Groundwater is pumped to

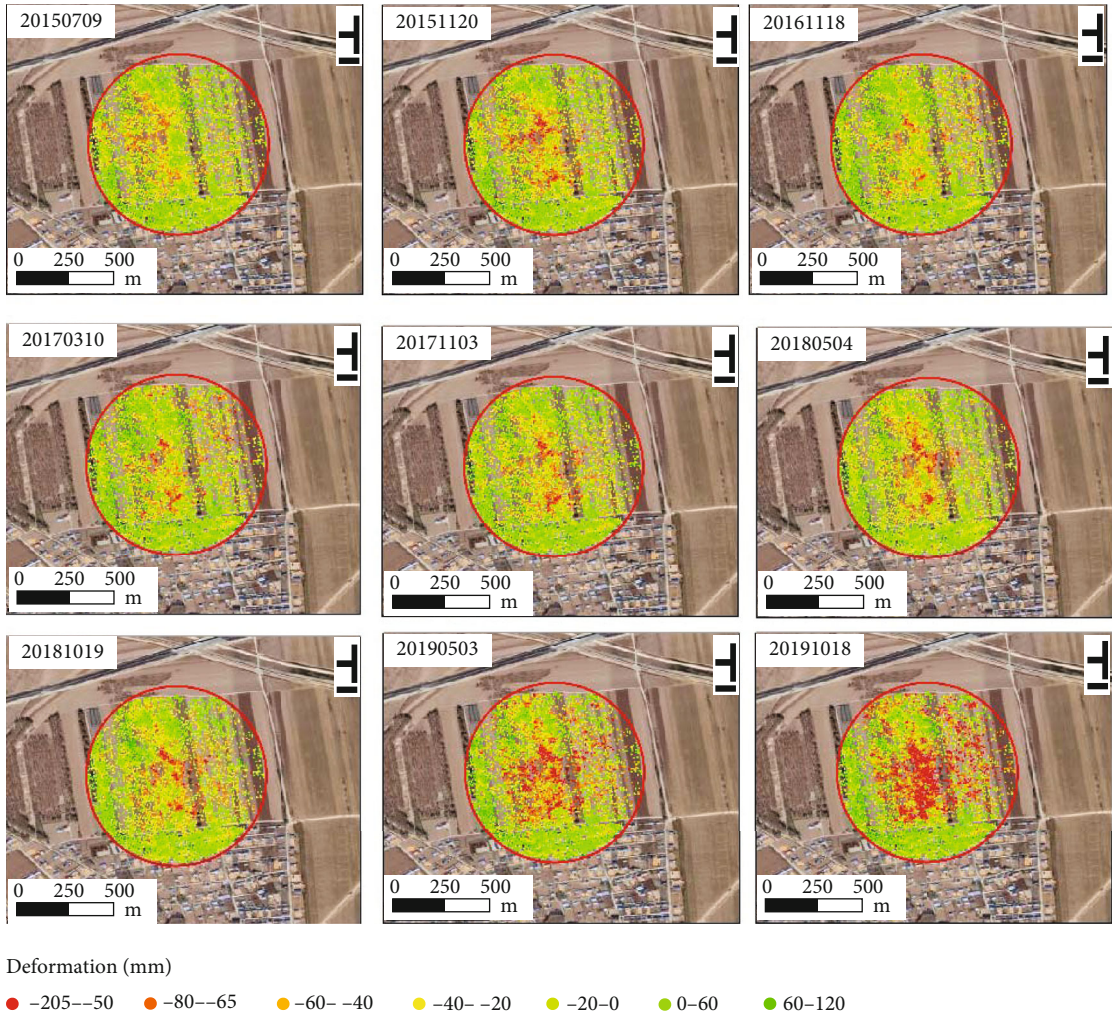

Figure 9: InSAR deformation map of oilfield regional time series.

irrigate the farmland and to accelerate the consolidation and subsidence of the soil [40]. Underground fluid and solute migrate in fractures [41]. In the rainy season, the farmland is irrigated by rainfall, and the rainfall also replenishes the groundwater. However, because of low precipitation of the study area, the corns in farmland need irrigation. Therefore, the rate of ground surface uplifting or subsidence in rainy season is significantly slowed. During the period from May to September 2017, a rainfall-abundant period, the ground surface rose significantly and then began to subside in the dry season, and the results in Figure 9 show that the area is still in a state of land subsidence by October 18, 2019, forming a sharp contrast with the oilfield area. This shows that the groundwater has been extracted by pumping wells, indicating that this is the main reason of farmland subsidence. Figures 10 and 11 were the UAV orthophotos and field survey in oilfields and farmland.

Both the oilfield area and farmland area have experienced several periodic stages of subsidence uplift, rather than continued subsidence. The period of subsidence in the oilfield area is long, while the time period of farmland subsidence represents seasonal changes. The overall performance is "subside in dry season and uplift in rainy season." The seasonal effect in the oilfield area is not obvious. Except for slight uplift, it has experienced a long period of subsidence time. Moreover, the layers exhibit different pore space structures and hydraulic properties due to grain size contrast [42]. This may also lead to different characteristics of land subsidence in different regions.

4.3. Subsidence Characteristics. The InSAR results in Figures 6 and 7 show that the subsidence rate in oilfields and farmland is stable. Even in two different landscape areas, the land preparation subsidence rate ranges of the two subsidence areas are relatively similar, ranging from 5.83 mm/a to -20.43 mm/a. The subsidence shape at the oilfield is approximately an oval, with a long axis diameter of 1.3 km and a short axis length of 0.55 km. This area is a saline soil land with poor coherence and fewer rate points, so only 402 subsidence points have been detected. The subsidence rates shown in Figures 6(b) and 6(c) are profiles of the subsidence area at the selection area. It can be observed from this section that the deformation rate gradually increases from the boundary to the middle of the area. The maximum

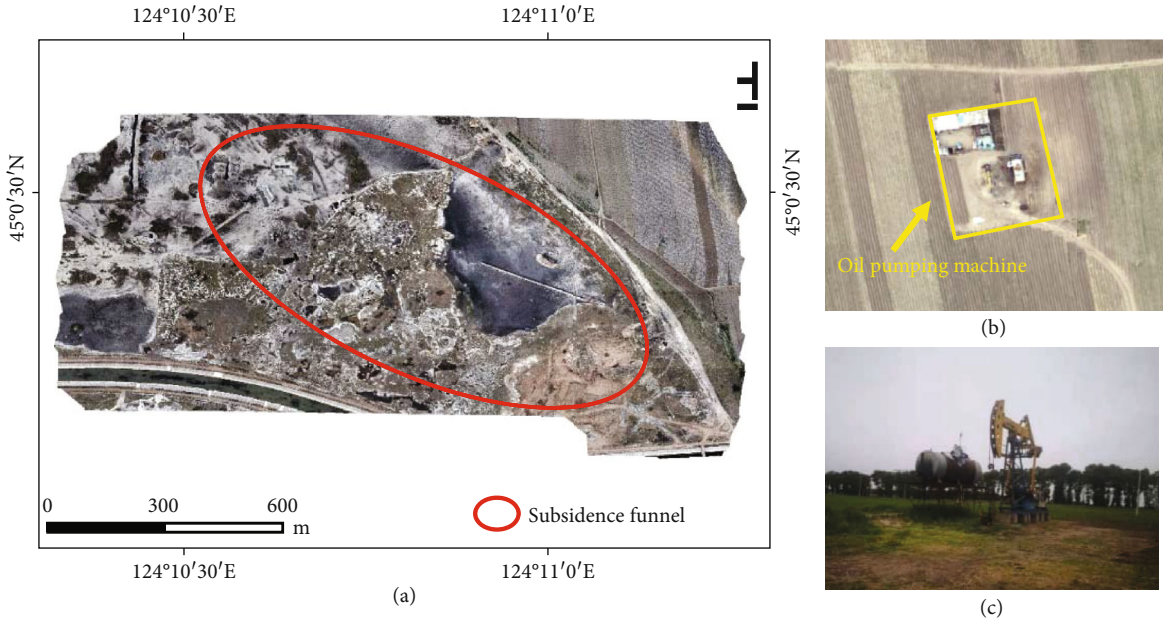

Figure 10: UAV and field survey. (a) UAV orthophoto in oilfield; (b) oil pumping well; (c) in situ photos of oil pumping.

deformation rate can reach -20.43 mm/a. The maximum deformation value is 136.12 mm, which is located in the center of the subsidence range, and the deformation rate decreases gradually on both sides. It conforms to the characteristics of the subsidence funnel. In Figures 7(b) and 7(c), the subsidence model selected at the farmland is approximately circular, with a diameter of 1.0 km. The subsidence rate ranges from 5.82 mm/a to -20.43 mm/a. This area has good coherence, and a total of 4115 coherent points were detected. Figure 7 is a cross-sectional view of the subsidence funnel. An obvious funnel shape can be seen from the scatter diagram and fitting curve of the two sections. Additionally, the maximum point of the A-A' profile deformation rate also reaches the maximum—20.43 mm/a.

Figure 10(a) shows the high-resolution optical of UAV in the settlement funnel of the oil field area. There is land subsidence around the pumping well funnel (Figure 10(b)). There are canals passing through the funnel in the south, and the surface elevation is significantly lower than the land on both sides. Figure 11(a) shows the high-resolution optical of UAV in the settlement funnel of farmland area. The surface conditions that cannot be clearly interpreted by optical remote sensing, such as pumping wells, can be interpreted by UAV high-resolution optical (Figure 11(b)). There are several water wells within the subsidence funnel, and the south of the funnel is residential land. Pumping groundwater from daily life may be the cause of land subsidence in this area.

5. Discussion

Land subsidence is a complex process, and its formation mechanism is related to the formation history, natural conditions, culture, and economy of the region. Both natural and human factors have influenced the area. In addition to oil pumping and water pumping, it may also be affected by tectonic activities, earthquake and other factors. Some properties of sediments and rock mass will affect the occurrence of land subsidence [43–46]. The study area is located in a plain area with open terrain and a large number of saline alkaline lake bubbles (Figure 4). Affected by the climate, the evaporation of bubbles in the lake causes the change in the water and soil environment and may also cause land subsidence. Figure 4 shows that there is indeed settlement around the lake bubble, but the settlement is distributed in a patchy manner and does not occur in a large area around the lake bubble. Therefore, the evaporation of the surface lake bubble will cause land subsidence to a certain extent, but it cannot become the main factor. Affected by tectonic activities, earthquakes occurred in the study area from July 2017 to August 2018. However, compared with the time-series box diagram in Figures 5(d) and 8(d), there is not much change in the overall subsidence law.

Therefore, the consolidation of natural sediments is the main natural cause of subsidence in the study area. Combined with the interpretation results of remote sensing images and the results of on-site UAV high-resolution optical, we find that the development of oil resources and the extraction of groundwater in the study area have also become the main man-made reasons in the area. The InSAR results show that the settlement in the study area is distributed in a patchy manner as a whole. Compared with the known studies on land subsidence in some cities [22, 23, 25], most of the land subsidence is uneven subsidence, that is, it is generally stable, and large-area subsidence occurs in one or several regions. Among those studies, the pumping of groundwater has become the main reason of ground subsidence, but the exploitation of groundwater in the study area is not concentrated in a certain area. UAV high-resolution optical confirmed that in the study area, water wells

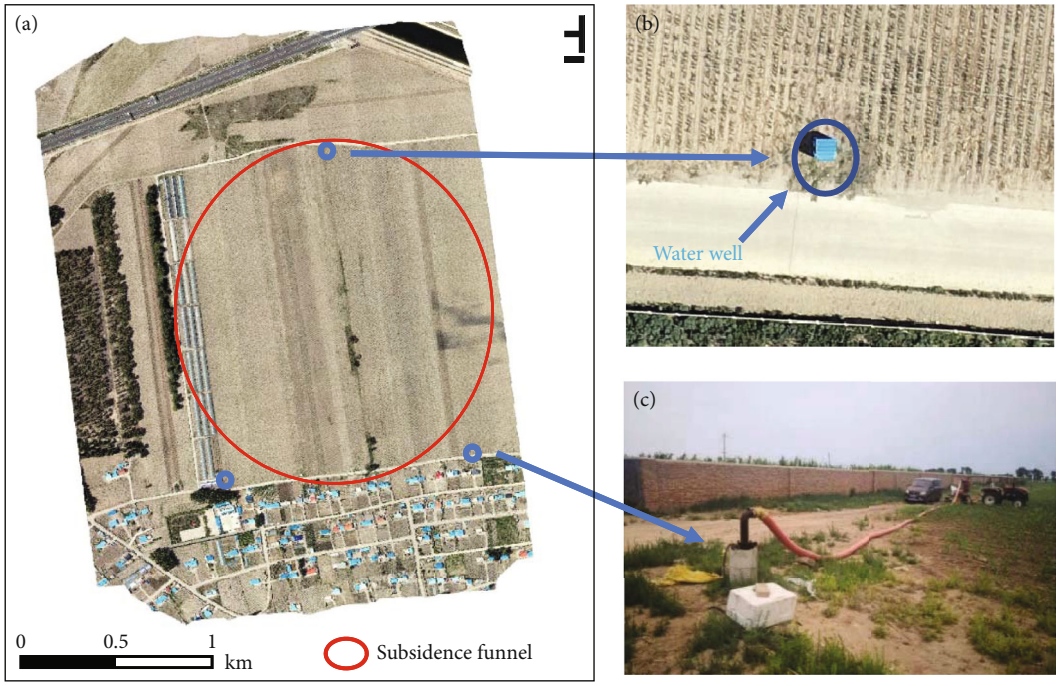

Figure 11: UAV and field survey. (a) UAV orthophoto in farmland; (b) groundwater pumping well; (c) in situ photos of groundwater pumping well.

are distributed around farmland for drinking and irrigation. Moreover, oil pumping wells are distributed around. This pumping engineering is distributed in point form, and leading land subsidence is characterized by patchy distribution.

In order to more clearly to explore the relationship between pumping and land subsidence, the production of Jilin Oilfield from 2015 to 2019 and the average cumulative subsidence of the corresponding year are selected to draw a scatter diagram and fit it [47]. According to the fitting results (Figure 12(a)), the oil field production is significantly correlated with the average cumulative settlement. This shows that pumping is the main cause of land subsidence in the oilfield area.

Figures 12(b) and 12(c) show the relationship between rainfall, evaporation, and buried depth of groundwater level of phreatic water and confined water in the study area in 2016 [48]. Affected by human activities, the confined water is in the stage of centralized mining from April to September. The water level drops and then recovers. Therefore, the surface subsidence and uplift in the rainy season will be affected to a certain extent. The phreatic water level changes obviously under the influence of rainfall and evaporation. From January to April, the rainfall is lower, the evaporation intensity is high, and the groundwater level drops. In May, the groundwater level increases with the increase in rainfall. In September, the rainfall decreases, and the water level drops. The change in groundwater level is similar to the trend of land subsidence in farmland.

The subsidence mechanism of farmland is schematic in Figure 13. The geological structure in the study area is relatively stable. The developed strata are mainly Cretaceous Neogene strata. The deformation rate through natural consolidation subsidence is usually less than 5 mm/a [49], while the maximum deformation rate in the study area can reach -22 mm/a. Additionally, the extraction of groundwater causes water-level depression [50], especially in the distribution area of underconsolidated or semiconsolidated soil layers, which will accelerate the process of consolidation and ground subsidence. Therefore, the extraction of groundwater may be the main cause of land subsidence in the study area. The time evolution results show that the subsidence has an elastic behavior along with seasonal changes; that is, the water level drops due to the extraction of groundwater in the dry season, and the support provided by pore pressure is transferred to the soil skeleton, resulting in the subsidence of the ground. The groundwater level is supplemented during rainfall [51].

On the other hand, the subsidence period of the oilfield is longer than that of farmland area, and there is no seasonal change, which may be caused by more complex reservoir pressure changes. However, the deformation value in oilfield is similar to that of farmland, indicating that both oil and water pumping cause ground subsidence. The burial depth of groundwater in the study area is generally 3-6 m, while the burial depth of pressure water is 25 m to 95 m [52]. The reservoir storage depth is 1518 m to 2072 m, with an average of 1800 m [53]. The land subsidence caused by groundwater pumping will be more obvious than that of oil pumping. Based on remote sensing interpretation, we confirm that there is less industrial development in this area, except in the oil well, and mainly in farmland, rural construction land, and grass land. Groundwater pumping wells are widely distributed, which can be used to irrigate farmland. Moreover, the farmland in this area was distributed

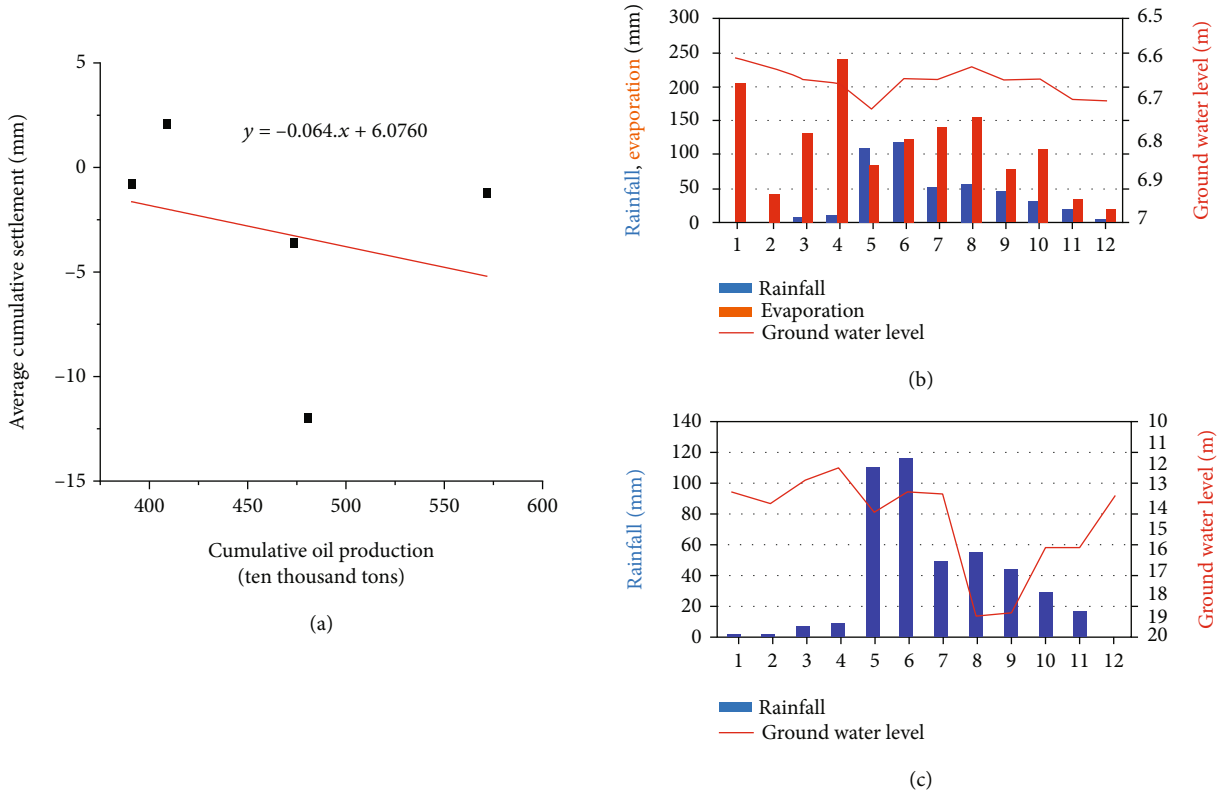

FIGURE 12: (a) Relationship between oilfield production and cumulative settlement. (b) Annual (2016) variation of rainfall and phreatic water level (Wang et al. 2020). (c) Annual (2016) variation of rainfall and groundwater level (Wang et al. 2020).

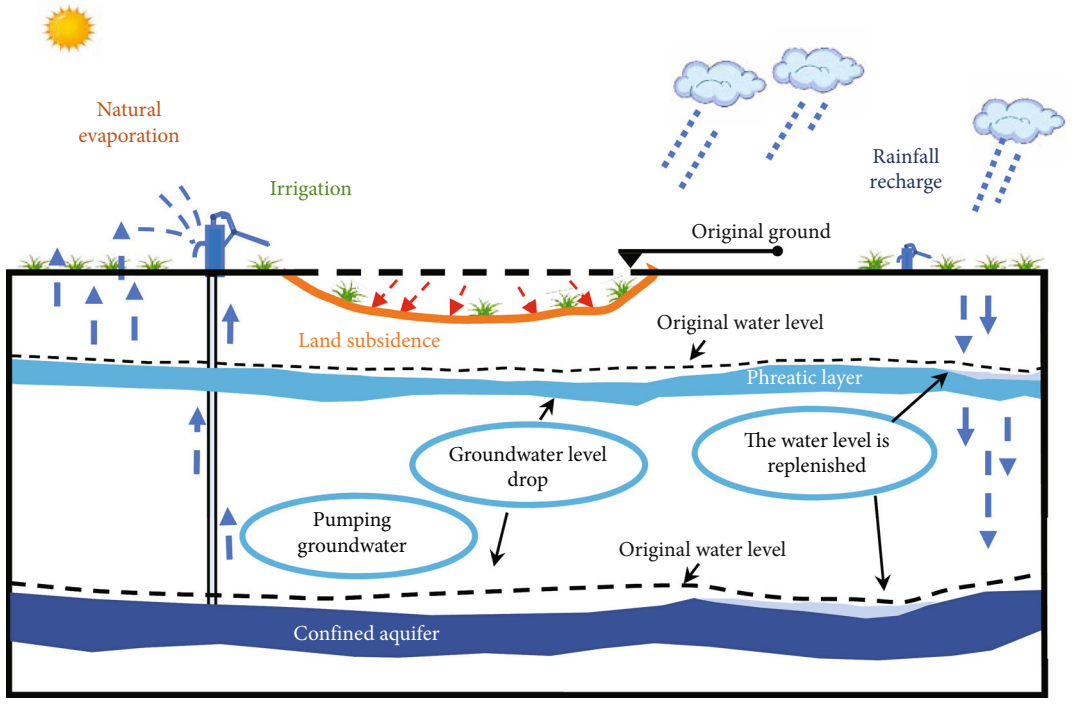

FIGURE 13: Schematic diagram of regional subsidence mechanism of farmland.

mostly in the study area. Therefore, it could be speculated that the reason for land subsidence in the study area is dominated by groundwater pumping, followed by oil extraction.

The subsidence mechanism of the oilfield is schematic in Figure 14. In the oilfield, the distribution of subsidence funnel is basically consistent with the boundary of the oilfield.

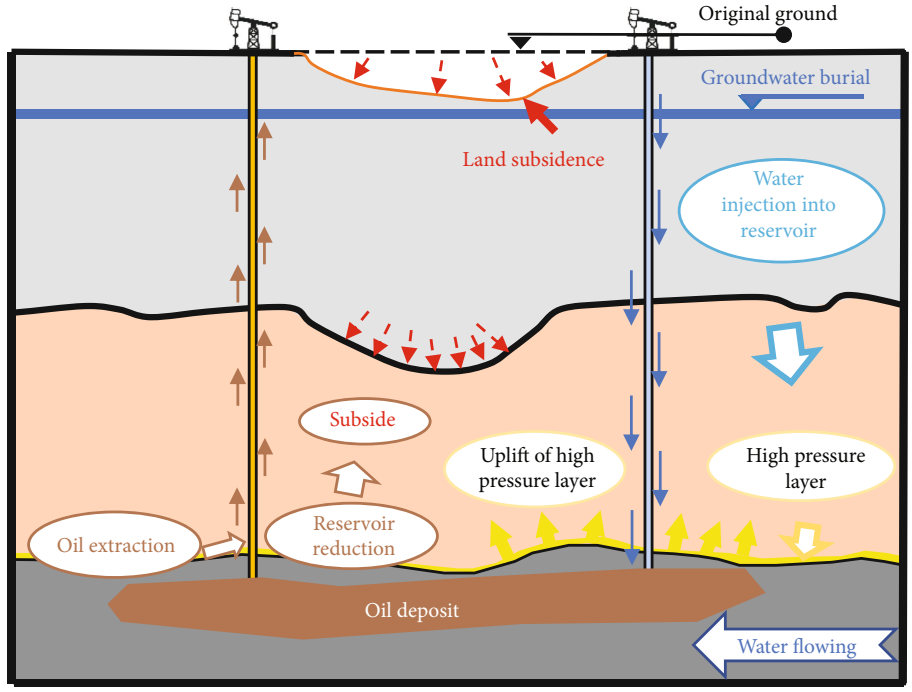

Figure 14: Schematic diagram of regional subsidence mechanism of oilfield.

However, from the position distribution of pumping wells, there is not much of an inevitable relationship with the position of subsidence funnel. Seen from Figure 4, areas where oil wells are concentrated, there is no result of subsidence funnel concentration. One subsidence funnel was also accompanied by several oil wells. The distribution position of pumping wells cannot represent the real distribution of underground oil storage scope. Moreover, due to the deep burial of underground oil and gas resources, the impact on the surface may not be fully reflected [54]. Oil production and the decline in groundwater level will cause local drainage in the upper part of the aquifer, release the pore pressure, destroy the stress structure of the original framework of the aquifer, produce compression deformation, and conduct it to the ground, resulting in ground deformation. Large-scale and high-intensity oil recovery may lead to stress release and variation deep underground and make local structures active, resulting in stratum dislocation and even shallow earthquakes, thus causing damage to mines, slopes, etc. [55]. Oil exploitation also brings people environmental problems that cannot be ignored. Oil exploitation reduces the underground pressure of the reservoir and causes reservoir compaction. When the compaction value reaches a certain order of magnitude, it will lead to surface subsidence.

6. Conclusions

The main purpose of this study is to analyze the characteristics of land subsidence in the western part of Songnen Plain by means of multisource remote sensing and analyze the relationship between land subsidence and the exploitation of groundwater and oil. A combination of optical remote sensing interpretation, InSAR analysis, and UAV high-resolution optical could help make this possible. This study used the western area of Songnen Plain as a case study and produced several findings, as below.

(1) The land subsidence in the western part of Songnen Plain is distributed in a porphyritic pattern, and the distribution of subsidence funnels is more concentrated in farmland areas than in oilfield areas. On the whole, the distribution range of subsidence funnels is basically consistent with that of pumping wells, while in the area with dense distribution of pumping wells, the distribution of the subsidence funnel is not dense. The distribution of the settlement funnel is spatially correlated with that of pumping wells, but not highly correlated

(2) Land subsidence in the western area of Songnen Plain is mainly caused by the exploitation of groundwater and oil. The long-term exploitation of groundwater causes uneven land subsidence, showing a trend of lifting in the dry season and decreasing in the rainy season. The groundwater is supplemented in the rainy season to help recover the surface elevation uplift. Oil pumping causes the oilfield area to be in a continuously subsiding state, which is not affected by the seasonal precipitation. During this period, due to water injection to the reservoir or to other reasons, this will cause short-term ground uplift and then continue to be in a subsiding state

(3) The extraction of underground fluid transfers the pressure that should be borne by water or oil to the soil skeleton, which increases and consolidates the effective stress of the soil layer, resulting in land

subsidence. There is no high correlation between the subsidence funnels and the range of the oil pumping area, but more are distributed in farmland areas. The dominant factor of land subsidence in western Songnen Plain is agricultural pumping irrigation. The groundwater level will be affected by rainfall and other factors. Rainfall not only supplies groundwater but also helps farmland irrigation. Rainfall alleviates the land subsidence in the western part of Songnen Plain to a certain extent

Data Availability

The data that support the findings of this study are available from the corresponding author, C.C., upon reasonable request.

Conflicts of Interest

The authors declare that they have no known competing financial interests or personal relationships that could have influenced the work reported in this paper.

Authors' Contributions

Lianjing Zheng contributes to data analysis and manuscript writing. Qing Wang is the project administration and provides useful advice for revising the manuscript. Zeyu Wang contributes to the remote sensing interpretation and making the figures. Fengyan Wang provides data and useful advices for revising the manuscript. Chen Cao contributes to conceptualization and supervision of the manuscript. All authors have read and approved the final manuscript.

Acknowledgments

This work was financially supported by the National Natural Science Foundation of China (Grant No.: 41820104001), the 2nd Research Announcement on the Earth Observations (EO-RA2) (Nos. ER2A2N114 and 2019.04-2022.04), and the Interdisciplinary Integration and Innovation Project of Jilin University (JLUXKJC2021ZZ17).

References

[1] K. Jin-Woo and L. Zhong, "Association between localized geohazards in West Texas and human activities, recognized by Sentinel-1A/B satellite radar imagery," *Scientific Reports*, vol. 8, no. 1, 2018.

[2] N. Q. Zhou, Y. Q. Tang, R. X. Lou, and S. M. Jiang, "Numerical simulation of deep foundation pit dewatering and land subsidence control of Xujiahui Metro Station," *Chinese Journal of Geotechnical Engineering*, vol. 33, pp. 1950–1956, 2011.

[3] Z. J. Luo, F. Zeng, and Y. Li, "Study on three-dimensional full coupling model of groundwater exploitation and land-subsidence control," *Journal of Jilin University*, vol. 39, pp. 1080–1086, 2009.

[4] H. Sun, D. Grandstaff, and R. Shagam, "Land subsidence due to groundwater withdrawal: potential damage of subsidence and sea level rise in southern New Jersey, USA," *Environmental Geology*, vol. 37, no. 4, pp. 290–296, 1999.

[5] S. J. Deverel and S. Rojstaczer, "Subsidence of agricultural lands in the Sacramento-San Joaquin Delta, California: role of aqueous and gaseous carbon fluxes," *Water Resources Research*, vol. 32, no. 8, pp. 2359–2367, 1996.

[6] A. Ustun, E. Tusat, and S. Yalvac, "Preliminary results of land subsidence monitoring project in Konya Closed Basin between 2006–2009 by means of GNSS observations," *Natural Hazards and Earth System Sciences*, vol. 10, no. 6, pp. 1151–1157, 2010.

[7] H. Fan, K. Deng, C. Ju, C. Zhu, and J. Xue, "Land subsidence monitoring by D-InSAR technique," *Mining Science & Technology*, vol. 21, no. 6, pp. 869–872, 2011.

[8] E. Chaussard, S. Wdowinski, E. Cabral-Cano, and F. Amelung, "Land subsidence in central Mexico detected by ALOS InSAR time-series," *Remote Sensing of Environment*, vol. 140, pp. 94–106, 2014.

[9] D. Massonnet, "Producing ground deformation maps automatically: the DIAPASON concept," in *Proceedings of the Geoscience & Remote Sensing, Igarss 97 Remote Sensing-a Scientific Vision for Sustainable Development*, Singapore, 1997.

[10] K. C. Lei, B. Chen, S. M. Jia, S. F. Wang, and Y. Luo, "Primary investigation of formation and genetic mechanism of land subsidence based on PS-InSAR technology in Beijing," *Spectroscopy & Spectral Analysis*, vol. 34, no. 8, pp. 2185–2189, 2014.

[11] R. F. Ulin, M. Taufik, and I. M. Anjasmara, "Application of PS-InSAR method for the land subsidence analysis using StaMPS (case study: Gresik Regency)," *IPTEK Journal of Proceedings Series*, no. 2, 2019.

[12] F. Kühn, A. Margane, T. Tatong, and T. Wever, "InSAR-based land subsidence map for Bangkok, Thailand," *zeitschrift für angewandte geologie*, vol. 50, no. 1, pp. 74–81, 2004.

[13] L. Li, M. Zhang, and K. Katzenstein, "Calibration of a land subsidence model using InSAR data via the ensemble Kalman filter," *Ground Water*, vol. 55, no. 6, pp. 871–878, 2017.

[14] J. Zhan, X. Qian, and C. Yan, "Monitoring the surface deformation of the Los Angeles using SBAS," *Engineering of Surveying and Mapping*, 2018.

[15] P. Farina, N. Casagli, and A. Ferretti, "Radar-interpretation of InSAR measurements for landslide investigations in civil protection practices," in *First North American Landslide Conference*, Vail, Colorado, USA, 2008.

[16] C. Cao, K. Zhu, T. Song et al., "Comparative study on potential landslide identification with ALOS-2 and sentinel-1A data in heavy forest reach, upstream of the Jinsha River," *Remote Sensing*, vol. 14, no. 9, p. 1962, 2022.

[17] M. Dehghani, M. Zoej, I. Entezam, A. Mansourian, and S. Saatchi, "InSAR monitoring of progressive land subsidence in Neyshabour, northeast Iran," *Geophysical Journal International*, vol. 178, no. 1, pp. 47–56, 2009.

[18] H. Sun, Q. Zhang, C. Zhao, C. Yang, Q. Sun, and W. Chen, "Monitoring land subsidence in the southern part of the lower Liaohe Plain, China with a multi-track PS-InSAR technique," *Remote Sensing of Environment*, vol. 188, pp. 73–84, 2017.

[19] C. Cao, W. Zhang, J. P. Chen, B. Shan, S. Y. Song, and J. W. Zhan, "Quantitative estimation of debris flow source materials by integrating multi-source data: a case study," *Engineering Geology*, vol. 291, article 106222, 2021.

[20] S. Bonvallot, J. L. Froger, D. Rémy, K. Bataille, and C. Robin, "Application of INSAR interferometry and geodetic surveys for monitoring Andean volcanic activity: first results from

ASAR-ENVISAT data," in *Proceedings of the International Symposium on the geodynamics of the Andes*, Barcelone, 2005.

[21] C. W. Lee, S. K. Lee, L. Zhong, and J. W. Kim, "Volcanic activity analysis of Mt. Sinabung in Indonesia using InSAR and GIS techniques," in *Proceedings of the Geoscience & Remote Sensing Symposium*, Milan, Italy, 2015.

[22] D. Zhou, A. S. Milas, J. Yu, L. Zhu, and N. Muhetaer, "Integrating RELAX with PS-InSAR technique to improve identification of persistent scatterers for land subsidence monitoring," *Remote Sensing*, vol. 12, no. 17, p. 2730, 2020.

[23] Z. Wang, J. Zhang, G. Huang, and Y. Zhang, "Monitoring land subsidence in Suzhou City using D-InSAR technique," in *Proceedings of the 2009 2nd International Congress on Image and Signal Processing*, Tianjin, China, 2009.

[24] P. E. Yastika, N. Shimizu, and H. Z. Abidin, "Monitoring of long-term land subsidence from 2003 to 2017 in coastal area of Semarang, Indonesia by SBAS DInSAR analyses using Envisat-ASAR, ALOS-PALSAR, and sentinel-1A SAR data," *Advances in Space Research*, vol. 63, no. 5, pp. 1719–1736, 2019.

[25] L. Yi, J. Wang, C. Shao, J. W. Guo, Y. Jiang, and B. Liu, "Land subsidence disaster survey and its economic loss assessment in Tianjin, China," *Natural Hazards Review*, vol. 11, pp. 35–41, 2010.

[26] F. E. Ikuemonisan, V. C. Ozebo, and O. B. Olatinsu, "Investigation of Sentinel-1-derived land subsidence using wavelet tools and triple exponential smoothing algorithm in Lagos, Nigeria," *Environmental Earth Sciences*, vol. 80, no. 21, 2021.

[27] K. Saylam, "Determining annual to decadal subsidence areas and rates using airborne Lidar, GPS surveys, and topographic maps at the wink sinkholes, West Texas," in *Proceedings of the GSA Annual Meeting 2019*, Portland, Oregon, 2021.

[28] Z. Mirzaii, M. Hasanlou, and J. Hatami, "Monitoring land subsidence in Azar Oilfield, Ilam, Iran through small-baseline SAR interferometry analysis," in *Proceedings of the IGARSS 2018-2018 IEEE International Geoscience and Remote Sensing Symposium*, Valencia, Spain, 2018.

[29] N. Fatholahi, M. Akhoondzadeh, and A. Bahroudi, "An investigation of surface deformation over oilfield in Southwest Iran (2003-2010) using InSAR and physical modelling," *International Journal of Remote Sensing*, vol. 41, no. 14, pp. 5355–5370, 2020.

[30] A. Edalat, M. Khodaparast, and A. M. Rajabi, "Scenarios to control land subsidence using numerical modeling of groundwater exploitation: Aliabad plain (in Iran) as a case study," *Environmental Earth Sciences*, vol. 79, no. 21, 2020.

[31] G. L. Cao, D. M. Han, and J. Moser, "Groundwater exploitation management under land subsidence constraint: empirical evidence from the Hangzhou-Jiaxing-Huzhou Plain, China," *Environmental Management*, vol. 51, no. 6, pp. 1109–1125, 2013.

[32] G. Y. Wang, D. Zhang, J. S. Feng, M. Z. Chen, and W. H. Shan, "Land subsidence due to deep groundwater withdrawal in northern Yangtze River Delta area," in *Proceedings of the 12th International IAEG Congress*, pp. 125–129, Torino, ITALY, Sep 15-19, 2014.

[33] Y. Aimaiti, F. Yamazaki, W. Liu, and A. Kasimu, "Monitoring of land-surface deformation in the Karamay oilfield, Xinjiang, China, using SAR interferometry," *Applied Sciences-Basel*, vol. 7, no. 8, p. 772, 2017.

[34] K. S. Rao, H. K. Al Jassar, N. J. Kodiyan, and V. P. Daniel, "Study on spatial variation of land subsidence over Minagish-Umm Gudair oil fields of Kuwait using synthetic aperture radar interferometry technique," *Journal of Applied Remote Sensing*, vol. 10, no. 1, p. 016026, 2016.

[35] N. A. A. Gido, H. Amin, M. Bagherbandi, and F. Nilfouroushan, "Satellite monitoring of mass changes and ground subsidence in Sudan's oil fields using GRACE and Sentinel-1 data," *Remote Sensing*, vol. 12, no. 11, p. 1792, 2020.

[36] W. Zhou, S. Li, J. Ke, and C. Gang, "InSAR application in detection of oilfield subsidence on Alaska North Slope," in *Proceedings of the Proceedings of the 41st US Symposium on Rock Mechanics (USRMS)*, Golden, Colorado, 2006.

[37] Y. Liu and H. J. Huang, "Characterization and mechanism of regional land subsidence in the Yellow River Delta, China," *Natural Hazards*, vol. 68, no. 2, pp. 687–709, 2013.

[38] N. Short, B. Brisco, N. Couture, W. Pollard, K. Murnaghan, and P. Budkewitsch, "A comparison of TerraSAR-X, RADARSAT-2 and ALOS-PALSAR interferometry for monitoring permafrost environments, case study from Herschel Island, Canada," *Remote Sensing of Environment*, vol. 115, no. 12, pp. 3491–3506, 2011.

[39] P. Berardino, G. Fornaro, R. Lanari, and E. Sansosti, "A new algorithm for surface deformation monitoring based on small baseline differential SAR interferograms," *IEEE Transactions on Geoscience & Remote Sensing*, vol. 40, no. 11, pp. 2375–2383, 2002.

[40] D. X. Vinh, "On the influence of the soil and groundwater to the subsidence of houses in Van Quan, Hanoi," *VNU Journal of Science: Earth and Environmental Sciences*, vol. 36, no. 4, 2020.

[41] Z. Dou, S. Tang, X. Zhang et al., "Influence of shear displacement on fluid flow and solute transport in a 3D rough fracture," *Lithosphere*, vol. 2021, no. Special 4, 2021.

[42] Z. Dou, Y. Liu, X. Zhang et al., "Influence of layer transition zone on rainfall-induced instability of multilayered slope," *Lithosphere*, vol. 2021, no. Special 4, 2021.

[43] A. Dc, A. Hc, Z. A. Wen, B. Jl, and S. B. Bo, "An analytical solution of equivalent elastic modulus considering confining stress and its variables sensitivity analysis for fractured rock masses," *Journal of Rock Mechanics and Geotechnical Engineering*, 2021.

[44] M. Z. Gao, J. Xie, J. Guo, Y. Q. Lu, Z. Q. He, and C. Li, "Fractal evolution and connectivity characteristics of mining-induced crack networks in coal masses at different depths," *Geomechanics and Geophysics for Geo-Energy and Geo-Resources*, vol. 7, no. 1, 2021.

[45] Y. Wang, H. N. Yang, J. Q. Han, and C. Zhu, "Effect of rock bridge length on fracture and damage modelling in granite containing hole and fissures under cyclic uniaxial increasing-amplitude decreasing-frequency (CUIADF) loads," *International Journal of Fatigue*, vol. 158, article 106741, 2022.

[46] C. Zhu, M. Karakus, M. C. He et al., "Volumetric deformation and damage evolution of Tibet interbedded skarn under multistage constant-amplitude-cyclic loading," *International Journal of Rock Mechanics and Mining Sciences*, vol. 152, p. 105066, 2022.

[47] Z. Kai, *Study on Ground Subsidence Regularity for Typical Oil Producing Region Based*, SBAS-InSAR JiLin University, 2022.

[48] W. Ya-nan, S. Yan-ling, and Z. Li-ling, "Analysis on the characteristics and causes of dynamic change of groundwater level in Qian'an County," *Jilin Geology*, vol. 39, 2020.

[49] S. Mazzotti, A. Lambert, M. Van der Kooij, and A. Mainville, "Impact of anthropogenic subsidence on relative sea-level rise

in the Fraser River delta," *Geology*, vol. 37, no. 9, pp. 771–774, 2009.

[50] S. Ghazali, "Relationship between level of water in Parishan Lake and surrounded wells with respect to excessive groundwater extraction," *Agricultural Economics Research*, vol. 4, no. 14, pp. 121–135, 2012.

[51] L. Damiba, A. Doumounia, V. Casey, A. Bounkoungou, and F. Zougmoré, "Analysis of rainfall variability on the groundwater levels of wells in the Nouaho Basin in East-Central Burkina Faso," *Water Resources and Protection*, vol. 12, no. 11, pp. 964–974, 2020.

[52] Y. Wang, "Analysis of hydrogeological characteristics and evaluation of groundwater resources in Qian'an County, Jilin Province," *Jilin Geology*, vol. 40, pp. 62–67, 2021.

[53] J. Wang, *Architecture and Remaining Oil Distribution Discipline of Sand Bodies of Gaotaizi Oil Layer in Qian'an Oilfield [PhD Thesis]*, China University of Petroleum (Beijing), Beijing, 2018.

[54] Y. Zhang, J. Tang, G. Li, and J. Teng, "Influence of depth-thickness ratio of mining on the stability of a bedding slope with its sliding surface in concave deformation," *International Journal of Mining Science and Technology*, vol. 26, no. 6, pp. 1117–1123, 2016.

[55] X. S. Li, Q. H. Li, Y. J. Hu et al., "Study on three-dimensional dynamic stability of open-pit high slope under blasting vibration," *Lithosphere*, vol. 2021, no. Special 4, article 6426550, 2022.